Same ligand, three first-row metals: comparing M-amido bifunctional reactivity (Mn, Fe, Co)

Matthew R Elsby, Scott y H Kim, Stephan N. Steinmann, R Tom Baker

COMMUNICATION

Same ligand, three first-row metals: Comparing M-amido bifunctional reactivity (Mn, Fe, Co)

Matthew R. Elsby, [a] Scott Y. H. Kim, [a] Stephan Steinmann,*, [b] and R. Tom Baker*, [a]

Received 00th January 20xx,
Accepted 00th January 20xx

DOI: 10.1039/x0xx00000x

The bifunctional reactivity of three metal SNS (bis)amido complexes was computationally assessed by comparing the nucelophilicity of the M–N$_{amido}$ donor (Mn, Fe, Co). Hirshfeld charges identified the Mn–N$_{amido}$ donor as most nucleophilic and Fe as most electrophilic metal. Reaction energy profiles of a model bifunctional H_2 activation showed Mn with the lowest reaction barrier (17 kcal/mol), followed by Fe and Co (21 and 29 kcal/mol).

Bifunctional ligands that enable multi-electron transformations through metal-ligand cooperation (MLC) have enhanced the performance of first-row transition metal catalysts.[1] Specifically, ligands that employ a Lewis base donor to facilitate E–H bond activation across an M–X bond are the most ubiquitous (**Scheme 1**) (E = H, B, Si; X = N, S, P, C).[2] This strategy is effective for challenging catalytic transformations including asymmetric hydrogenation,[3] transfer hydrogenation,[4] hydrogen formation and oxidation,[5] hydroborations,[6] hydrosilylations,[7] and (acceptorless) dehydrogenative couplings of a broad scope of organics.[8] Over the past decade, numerous ligand sets of varying donor combinations (C, N, O, P, S)[7c, 9] and hapticities (classic tridentate pincer *vs*. bi/ tetradentate) have been employed to facilitate these reactions. While the boundaries of ligand design are being continually pushed to expand the catalytic scope of these reaction pathways, there has been less evaluation of how the selected base metal influences the reactivity of these bifunctional ligands.

The Szymczak group reported the divergent reactivity of a series of analogous complexes across the first-row (V, Mn, Fe, Co, Zn) for hydrazine capture and N–N bond cleavage.[10] [11] They found that while all complexes are capable of capturing hydrazine,

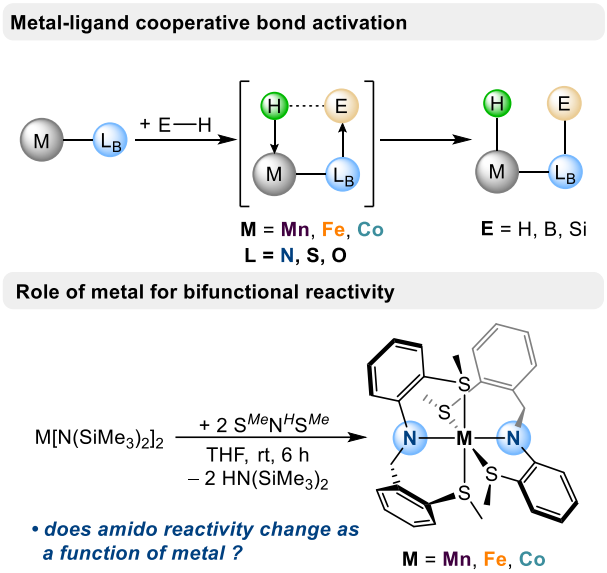

Scheme 1. [Top] General mechanism of metal-ligand cooperative E–H bond activation; [Bottom] Synthesis of M[S^{Me}NS^{Me}]$_2$ complexes.

subsequent N–N bond reduction does not occur with the Mn and Zn analogues; with Fe and Co being most active. Relatedly, Kirchner[12] and Mezzetti[13] have both contributed to the comparison of isostructural and isoelectronic Mn(I) and Fe(II) bifunctional catalysts for (de)hydrogenations. Finally, a recent work performed a DFT investigation on the barrier for bifunctional H_2 activation with Lewis acid tris(phosphino)borane complexes across the first-row metals.[14] These formative works bring to the forefront the need for further systematic comparison of bifunctional complexes across the base metals. This will offer insight towards the design of catalysts capable of more challenging bond activations (C–H, C–N, N–N).[1d, 2b]

Our group has developed a library of complexes across the first-row metals (Mn to Cu) featuring a bifunctional [S^{Me}NS^{Me}] (**L**) ligand, and have reported their capacity for MLC catalysis.[15] Key design features of **L** include a Lewis basic amido donor and a hemilabile thioether donor to allow for a vacant coordination site. We have

[a] *Department of Chemistry and Biomolecular Sciences and Centre for Catalysis Research and Innovation, University of Ottawa, Ottawa, Ontario, K1N 6N5 Canada. Email: rbaker@uottawa.ca*
[b] *Univ Lyon, ENS de Lyon, CNRS UMR 5182, Université Claude Bernard Lyon 1, Laboratoire de Chimie, Lyon, France. Email : stephan.steinmann@ens-lyon.fr*
† Electronic Supplementary Information (ESI) available: Synthetic procedures and NMR data. Computational details and Cartesian coordinates of all structures. Calculated Hirshfeld charges, Fukui indices, and molecular orbitals. Crystallographic details for **Co1**. See DOI: 10.1039/x0xx00000x

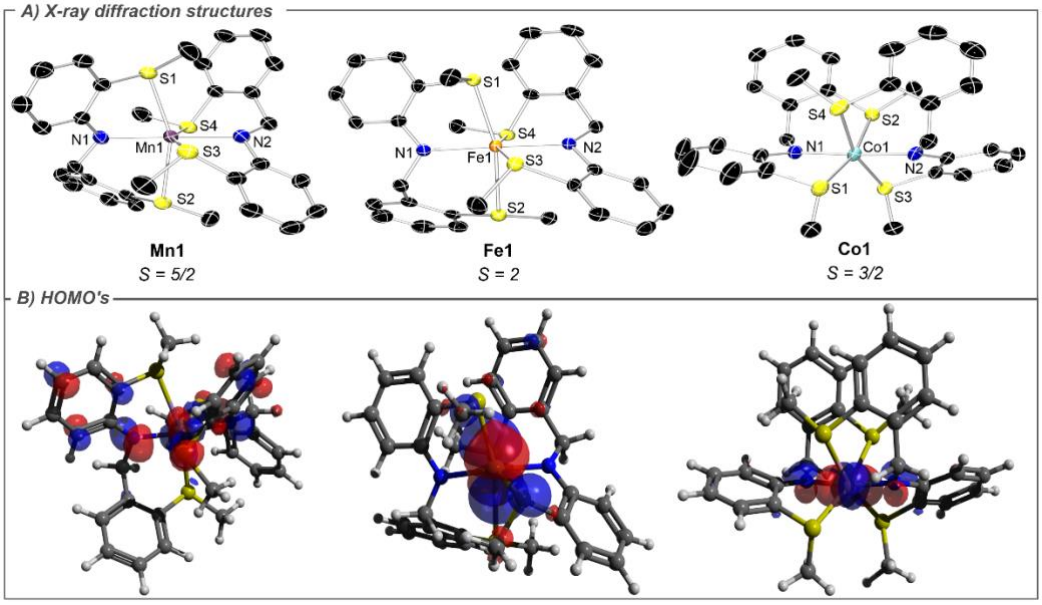

Figure 1. A) Solid-state molecular depictions of **Mn1**, **Fe1**, and **Co1**. Thermal ellipsoids are shown at 50% probability and hydrogen atoms are removed for clarity. Selected bond lengths (Å): Mn(1)–N(1) 2.099(2); Mn(1)–N(2) 2.122(2); Fe(1)–N(1) 2.015(2); Fe(1)–N(2) 2.031(2); Co(1)–N(1) 1.967 (2); Co(1)–N(2) 1.974(2); B) Highest occupied molecular orbitals.

obtained three analogous M($S^{Me}NS^{Me}$)$_2$ complexes (M = Mn, Fe, Co) by reaction of the appropriate M[N($SiMe_3$)$_2$]$_2$ complex with two equiv. of HL to afford the desired complexes **Mn1**,[15d] **Fe1**,[15b] and **Co1**[15c] (**Scheme 1**). This provided a rare opportunity to directly examine identical analogues of bifunctional complexes. Herein, we describe our efforts to compare these three compounds computationally, and to evaluate a bifunctional H_2 activation reaction profile to discern reactivity patterns amongst the metals within our [SNS]-ligand platform to aid in design of next generation catalysts.

We began our investigation by first determining the potential ground state of these divalent complexes. All calculations were carried out with the M06L functional and geometry optimization and frequency calculations were performed with the def2-SVP basis set.[16] Energies of the optimized structures were revaluated by additional single-point calculations on each optimized geometry using the triple-ζ basis set def2-TZVP with solvation energies in THF accounted for using the self-consistent reaction field (SCRF) approach.[17] It was found that complexes **Mn1**, **Fe1**, and **Co1** display respectively a sextet, quintet, and quartet ground state, preferentially adopting a high-spin configuration (See Table S15 in ESI†). This is attributed to the presence of the 'hard' amido donors and four weak-field thioether donors around the metal centre. Solution state magnetic measurements using Evans's method gave values of μ_B = 6.0, 4.9, and 3.8 for **Mn1**, **Fe1**, and **Co1**, respectively, corroborating the DFT assigned ground-states. The metrical parameters of the DFT optimized structures match well with experimental bond lengths from single-crystal X-ray diffraction (SCXRD) experiments (**Figure 1A** and Tables S3-S5 in ESI†). A definite contraction of the M–N bonds is seen moving from Mn to Co, with an average decrease across both metal-amido bonds of 0.083 and 0.053 Å from Mn to Fe, and Fe to Co, respectively. Furthermore, the relative orientation of the meridional **L** ligands around the metal centre also changes in the solid-state; both **Mn1** and **Fe1** display unsymmetrical **L** coordination, while **Co1** exhibits pseudo C_2 symmetry.[18]

The optimized geometries were used to evaluate molecular orbital (MO) character and frontier molecular orbitals (FMO) (Figures S11-S13 in ESI†). The calculated HOMO-LUMO gaps for the three complexes are 2.74, 3.03, and 2.99 eV for **Mn1**, **Fe1**, and **Co1**, respectively. While the LUMO is highly delocalized across the ligand aromatic system for all three complexes, there is divergence in the HOMOs (**Figure 1B**). The HOMO of **Mn1** is distributed amongst both amido donors and their respective aromatic framework, as well as the Mn centre. That of **Fe1** is nearly exclusively based on the Fe centre while the HOMO of symmetric **Co1** is distributed amongst the metal and both amido nitrogens.

Base-metal complexes that bear bifunctional amine/amido moieties are well established as effective electrocatalysts for H_2 oxidation and formation.[19] As such, cyclic voltammetry studies were performed under N_2 to probe electrochemical activity (See ESI†). The cyclic voltammogram of **Fe1** in dichloromethane solution shows a quasi-reversible oxidation at $E_{1/2}$ = –0.54 V, versus $Cp_2Fe^{+/0}$ at a scan rate of 100 mV/s. Given the large metal character of the **Fe1** HOMO, this event is attributed to the Fe^{II}/Fe^{III} redox couple. Scanning to more positive potentials revealed two additional irreversible oxidations at 0.11 and 0.56 V, attributed to oxidation of the amido ligands. Under the same conditions, **Co1** displays a quasi-reversible oxidation at $E_{1/2}$ = –0.43 V, as well as two irreversible oxidations at 0.32 V and 0.68 V. Given the significant metal character of the **Co1** HOMO, the reversible event is assigned as the Co^{II}/Co^{III} redox couple, while the irreversible events are also likely a result of oxidation of both amido ligands. Finally, the cyclic voltammogram of **Mn1** showed no activity within the probed voltage range.

Fukui indices were calculated to assess the three bis(amido) complexes for bifunctional reactivity as a function of amido nucleophilicity and metal electrophilicity; similar to the critical design of frustrated Lewis pairs[20] (Tables S12-S14 in ESI†). While the

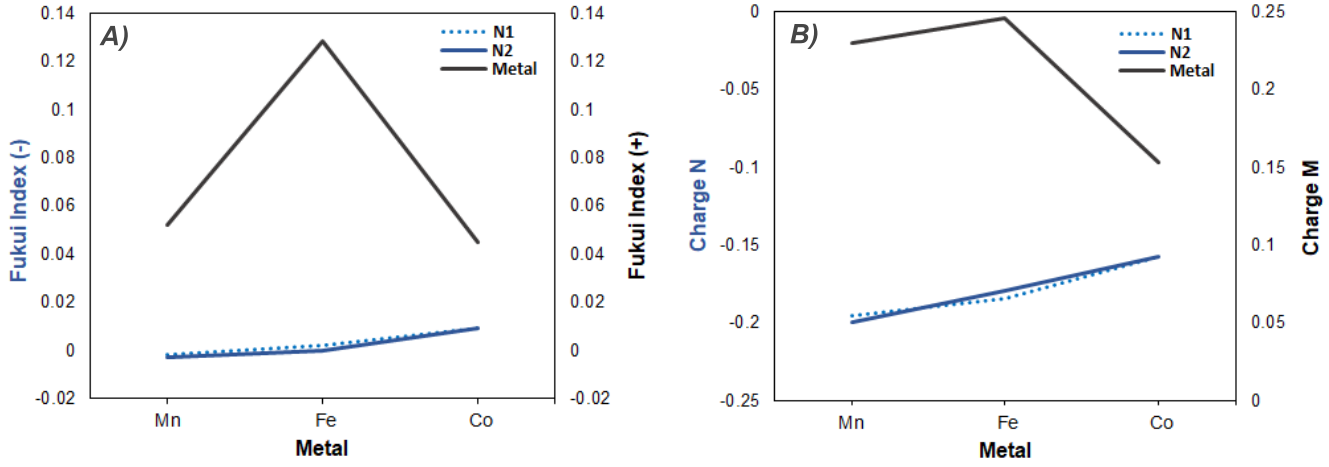

C)	Mn	Fe	Co	Mn-N1	Mn-N2	Fe-N1	Fe-N2	Co-N1	Co-N2
Hirshfeld	0.2304	0.245654	0.15347	-0.19562	-0.19925	-0.18416	-0.17939	-0.15732	-0.15734
Fukui (+)	0.05195	0.12836	0.04479						
Fukui (-)				-0.0019	-0.0026	0.00217	0.0003	0.0093	0.00928

Figure 2. A) Chart of calculated Fukui (-/+) indices for both amido donors and metal of **Mn1**, **Fe1**, and **Co1**; B) Calculated Hirshfeld charges for both amido donors and metals; C) Table of Hirshfeld charges and Fukui indices shown in A and B.

differences in Fukui indices are small (**Figure 2A**), there is an upward linear trend in the amido nucleophilicity moving from Mn to Co. In contrast, a non-monotonic trend is found for the electrophilicity, with Fe being the most electrophilic. Alternatively, Hirshfeld charges can also be used to quantify nucleophilicity/electrophilicity.[21] The calculated values (**Figure 2B**) offer more numerical contrast between the three complexes and are also in opposition to the trends suggested by the Fukui indices (Tables S9-S11 in ESI†). While Fe remains the most electrophilic, the Hirshfeld charges suggest that Mn–N_{amido} donors are the most nucleophilic, as opposed to Co–N_{amido}.

To learn which parameter more accurately predicts reactivity trends in our system, the potential energy surface of a simple outer-sphere H–H activation across the M–N_{amido} bond was evaluated for the three ML_2 complexes (**Figure 3**). The first step is dissociation of one of the hemilabile thioether donors of the 6-membered ring to yield a 5-coordinate species (**M2**) with a vacant coordination site for substrate activation. Previous work with **Mn1** and **Fe1** has established the validity of these proposed species,[15b, 15d] and the

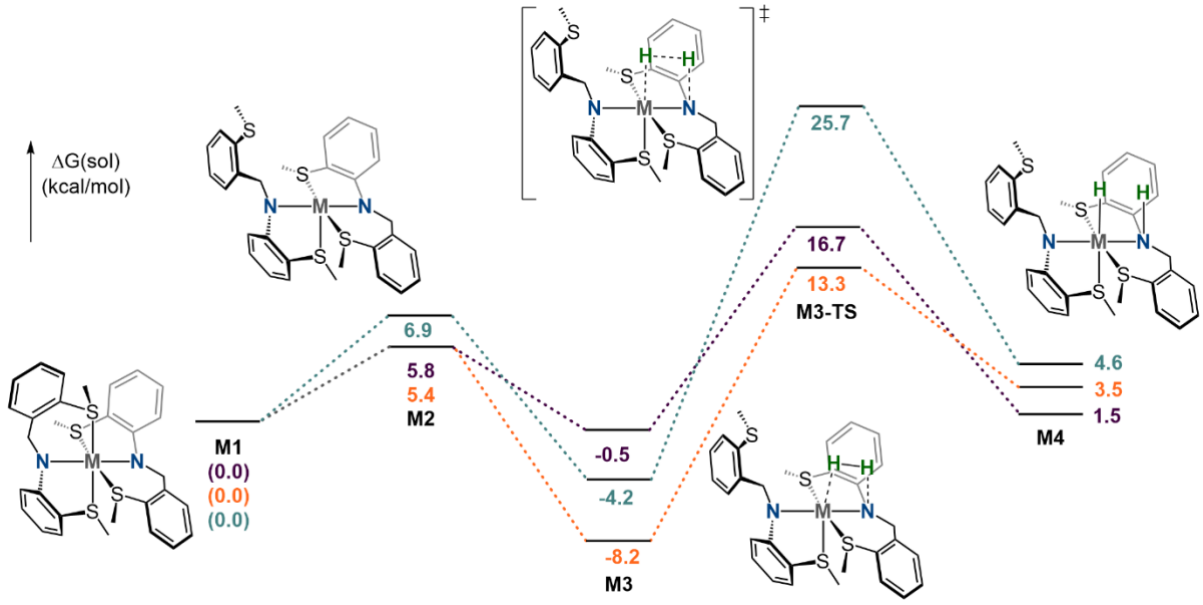

Figure 3. Energy reaction profile for H_2 activation across M–N_{amido} bond in **Mn1** (purple), **Fe1** (orange), and **Co1** (teal).

energies for the three 5-coordinate species (**M2**) are nearly isoenergetic about 5-7 kcal/mol above their 6-coordinate precursors. Direct interaction of H_2 with the M–N bond of the κ^3-[$S^{Me}NS^{Me}$] ligand forms **M3**, similar to previous work by Morris.[22] It should be noted that attempts to calculate a dihydrogen intermediate resulted in optimization towards the **M3** species. The energies diverge here, with Fe being most exergonic at -8.2 kcal/mol, followed by Co and Mn at -4.2 and -0.5 kcal/mol, respectively. While heterolytic H–H cleavage through **M3-TS** shows the Fe pathway as the lowest energy TS, it is in fact the Mn pathway that has the lowest activation barrier at 17.2 kcal/mol, followed by Fe and Co with barriers of 21.5 and 29.9 kcal/mol, respectively. Upon arriving at the final metal-hydride species **M4**, the energies realign, with the final Mn product being lowest in energy. As tested by single-point energy evaluations based on the M06-L geometries, these reactivity trends are faithfully reproduced by a wide range of functionals (Figures S15-S20 in ESI).

Contextually, the Hirshfeld charges which predicted the Mn–N_{amido} as the most nucleophilic may provide a more accurate theoretical depiction for predicting reactivity than the Fukui indices. The calculated DFT reaction profile indicates that bifunctional addition of H_2 to all three complexes is energetically accessible, but it is **Mn1**, which has the most nucleophilic amido, that proceeds through the lowest energy barrier. This is followed by **Fe1** which has the second highest amido nucleophilicity, and also most electrophilic metal. While this may initially indicate that amido nucleophilicity is a more significant factor, it should be noted that Mn is nearly as electrophilic as Fe (0.230 and 0.245 respectively), while the respective amido donors exhibit a greater difference in nucleophilicity (-0.199 and -0.179). This suggests that optimizing a careful balance of these two properties – a nucleophilic Lewis base to accept a proton and an electrophilic metal to accept a hydride – is required to provide the lowest energy barrier pathway. This indeed supports previous findings in our lab, whereby **Mn1** has been found to be the best performing and long-lasting catalyst in related reductive transformations.[15d]

To provide experimental context to the DFT results, reactions of each individual complex with dihydrogen were performed. A THF solution of the appropriate complex (**Mn1**, **Fe1**, or **Co1**) was charged to a J. Young tube. The nitrogen atmosphere was removed and 1 atm of H_2 was subsequently added. Addition of H_2 to either **Co1** or **Fe1** resulted in no color change or change in the ^{1}H NMR spectrum. Upon heating either of these solutions to 60 °C, a color change was initially observed after 5 minutes followed by rapid decomposition as evidenced by formation of black precipitates. Alternatively, addition of H_2 to **Mn1** at room temperature resulted in a color change from yellow to a light brown. The resultant ^{1}H NMR spectrum was uninformative due to weak peak shifting (typical of Mn(II) complexes) and overlap with *proteo*-THF resonances. However, the isotropic EPR spectrum provided evidence of speciation to a new paramagnetic product. The initial room temperature EPR spectrum of **Mn1** shows a sextet at g = 2.01 with α = 70 G from coupling to *I* = 5/2 ^{59}Mn. Upon reaction with H_2, this hyperfine coupling disappears to yield a single broad feature at g = 2.04 (Figure S2 in ESI). Finally, to investigate the potential reactivity of this paramagnetic species, a solution of benzaldehyde and 20 mol% **Mn1** in benzene-d_6 was charged with dihydrogen. A color change from yellow to beige was observed and the crude ^{1}H NMR showed the appearance of benzyl alcohol product, demonstrating the ability of this species to transfer hydrogen.

These experimental results corroborate well with our DFT reaction profiles, whereby only **Mn1**, which has an activation barrier of 17.2 kcal/mol, provided evidence of facile reactivity with dihydrogen. While the relationship of reactivity to the Hirshfeld charge has a positive correlation, further work across a broader scope of known bifunctional complexes may firmly establish this trend. The results described herein will influence future catalyst design with our [SNS] ligand set to try and achieve this balance between metal and bifunctional Lewis base donor by varying alternate ancillary ligands at the metal.

We thank the NSERC (Discovery Grant 2019-05959) for generous operating support and the University of Ottawa, Canada Foundation for Innovation, and Ontario MEDI for essential infrastructure. MRE acknowledges receipt of an Ontario Graduate Scholarship. SYHK acknowledges the CIC Inorganic Chemistry Exchange program.

Author Contributions

MRE performed DFT calculations with the assistance of SS and wrote the manuscript. SYHK performed electrochemical studies. SS and RTB helped write the manuscript.

Conflicts of interest

There are no conflicts to declare.

Notes and References

(1)(a)J. I. van der Vlugt, *Eur. J. Inorg. Chem.*, 2012, **2012**, 363-375; (b)J. R. Khusnutdinova and D. Milstein, *Angew. Chem. Int. Ed.*, 2015, **54**, 12236-12273; (c)R. H. Morris, *Acc. Chem. Res.*, 2015, **48**, 1494-1502; (d)M. R. Elsby and R. T. Baker, *Chem. Soc. Rev.*, 2020, **49**, 8933-8987; (e)T. Zell and D. Milstein, *Acc. Chem. Res.*, 2015, **48**, 1979-1994; (f)Y.-Y. Li, S.-L. Yu, W.-Y. Shen and J.-X. Gao, *Acc. Chem. Res.*, 2015, **48**, 2587-2598.

(2)(a)L. Alig, M. Fritz and S. Schneider, *Chem. Rev.*, 2018, **119**, 2681-2751; (b)T. Higashi, S. Kusumoto and K. Nozaki, *Chem. Rev.*, 2019, **119**, 10393-10402.

(3)(a)P. O. Lagaditis, P. E. Sues, J. F. Sonnenberg, K. Y. Wan, A. J. Lough and R. H. Morris, *J. Am. Chem. Soc.*, 2014, **136**, 1367-1380; (b)M. Garbe, K. Junge, S. Walker, Z. Wei, H. Jiao, A. Spannenberg, S. Bachmann, M. Scalone and M. Beller, *Angew. Chem. Int. Ed.*, 2017, **56**, 11237-11241; (c)M. B. Widegren, G. J. Harkness, A. M. Slawin, D. B. Cordes and M. L. Clarke, *Angew. Chem. Int. Ed.*, 2017, **56**, 5825-5828.

(4)(a)M. Pang, J.-Y. Chen, S. Zhang, R.-Z. Liao, C.-H. Tung and W. Wang, *Nat. Commun.*, 2020, **11**, 1-9; (b)W. Zuo, A. J. Lough, Y. F. Li and R. H. Morris, *Science*, 2013, **342**, 1080-1083; (c)K. Z. Demmans, M. E. Olson and R. H. Morris, *Organometallics*, 2018, **37**, 4608-4618; (d)L. De Luca, A. Passera and A. Mezzetti, *J. Am. Chem. Soc.*, 2019, **141**, 2545-2556; (e)A. Zirakzadeh, S. R. de Aguiar, B. Stöger, M. Widhalm and K. Kirchner, *ChemCatChem*, 2017, **9**, 1744-1748.

(5)(a)M. L. Helm, M. P. Stewart, R. M. Bullock, M. R. DuBois and D. L. DuBois, *Science*, 2011, **333**, 863-866; (b)T. Liu, D. L. DuBois and R. M. Bullock, *Nat. Chem.*, 2013, **5**, 228-233; (c)E. B. Hulley, N. Kumar, S. Raugei and R. M. Bullock, *ACS Catal.*, 2015, **5**, 6838-6847.
(6)(a)C. Ghosh, S. Kim, M. R. Mena, J.-H. Kim, R. Pal, C. L. Rock, T. L. Groy, M.-H. Baik and R. J. Trovitch, *J. Am. Chem. Soc.*, 2019, **141**, 15327-15337; (b)C. Erken, A. Kaithal, S. Sen, T. Weyhermüller, M. Hölscher, C. Werlé and W. Leitner, *Nat. Commun.*, 2018, **9**, 1-9; (c)J. Liu, J.-Y. Chen, M. Jia, B. Ming, J. Jia, R.-Z. Liao, C.-H. Tung and W. Wang, *ACS Catal.*, 2019, **9**, 3849-3857.
(7)(a)S. N. MacMillan, W. H. Harman and J. C. Peters, *Chem. Sci.*, 2014, **5**, 590-597; (b)M. A. Nesbit, D. L. Suess and J. C. Peters, *Organometallics*, 2015, **34**, 4741-4752; (c)M. R. Elsby and R. T. Baker, *Chem. Commun.*, 2019, **55**, 13574-13577.
(8)(a)J. s. A. Luque-Urrutia, M. Solà, D. Milstein and A. Poater, *J. Am. Chem. Soc.*, 2019, **141**, 2398-2403; (b)U. K. Das, S. Chakraborty, Y. Diskin-Posner and D. Milstein, *Angew. Chem. Int. Ed.*, 2018, **57**, 13444-13448; (c)S. Chakraborty, P. Daw, Y. Ben David and D. Milstein, *ACS Catal.*, 2018, **8**, 10300-10305.
(9)(a)S. Fu, Z. Shao, Y. Wang and Q. Liu, *J. Am. Chem. Soc.*, 2017, **139**, 11941-11948; (b)A. Dubey, L. Nencini, R. R. Fayzullin, C. Nervi and J. R. Khusnutdinova, *ACS Catal.*, 2017, **7**, 3864-3868; (c)A. Dubey, S. W. Rahaman, R. R. Fayzullin and J. R. Khusnutdinova, *ChemCatChem*, 2019, **11**, 3844-3852; (d)H. Song, K. Ye, P. Geng, X. Han, R. Liao, C.-H. Tung and W. Wang, *ACS Catal.*, 2017, **7**, 7709-7717; (e)L. T. Scharf, A. Kowsari, T. Scherpf, K.-S. Feichtner and V. H. Gessner, *Organometallics*, 2019, **38**, 4093-4104.
(10)J. J. Kiernicki, M. Zeller and N. K. Szymczak, *J. Am. Chem. Soc.*, 2017, **139**, 18194-18197.
(11)J. J. Kiernicki, M. Zeller and N. K. Szymczak, *Inorg. Chem.*, 2020, **59**, 9279-9286.
(12)N. Gorgas and K. Kirchner, *Acc. Chem. Res.*, 2018, **51**, 1558-1569.
(13)A. Passera and A. Mezzetti, *Adv. Synth. Catal.*, 2019, **361**, 4691-4706.
(14)P. Su, Y. Li and Z. Ke, *Chem Asian J.*, 2021.
(15)(a)M. R. Elsby, K. Ghostine, U. K. Das, B. M. Gabidullin and R. T. Baker, *Organometallics*, 2019, **38**, 3844-3851; (b)U. K. Das, S. L. Daifuku, T. E. Iannuzzi, S. I. Gorelsky, I. Korobkov, B. Gabidullin, M. L. Neidig and R. T. Baker, *Inorg. Chem.*, 2017, **56**, 13766-13776; (c)B. Fitchett. **2018**, Université d'Ottawa/University of Ottawa Masters Thesis; (d)M. R. Elsby, M. Son, C. Oh, J. Martin, M.-H. Baik and R. T. Baker, *ACS Catal.*, 2021, **11**, 9043-9051.
(16)(a)Y. Zhao and D. G. Truhlar, *J. Chem. Phys.*, 2006, **125**, 194101; (b)F. Weigend and R. Ahlrichs, *Phys. Chem. Chem. Phys.*, 2005, **7**, 3297-3305.
(17)B. Marten, K. Kim, C. Cortis, R. A. Friesner, R. B. Murphy, M. N. Ringnalda, D. Sitkoff and B. Honig, *J. Phys. Chem.*, 1996, **100**, 11775-11788.
(18)The three different conformers of **Mn1**, **Fe1**, and **Co1** were also calcualted with each metal and the energies were compared. While both Fe, and Co were approx 4 kcal/mol lower in energy adopting the Mn conformer, subsequent examination of the H_2 reaction pathway gave higher energy reaction intermediates than their respective original conformations.
(19)(a)R. M. Bullock and M. L. Helm, *Acc. Chem. Res.*, 2015, **48**, 2017-2026; (b)E. B. Hulley, K. D. Welch, A. M. Appel, D. L. DuBois and R. M. Bullock, *J. Am. Chem. Soc.*, 2013, **135**, 11736-11739.
(20)(a)D. W. Stephan and G. Erker, *Angew. Chem. Int. Ed.*, 2015, **54**, 6400-6441; (b)T. A. Rokob and I. Papai, in *Frustrated Lewis Pairs I*, 2013 pp. 157-211.
(21)S. Liu, *J. Phys. Chem. A*, 2015, **119**, 3107-3111.
(22)C. S. Seo, B. T. Tsui, M. V. Gradiski, S. A. Smith and R. H. Morris, *Catal. Sci. Technol.*, 2021, **11**, 3153-3163.

Table of Contents Only